Novel Triclosan-Bound Hybrid-Silica Nanoparticles and their Enhanced Antimicrobial Properties

*Igor Makarovsky, Yonit Boguslavsky, Maria Alesker, Jonathan Lellouche, Ehud Banin, and Jean-Paul Lellouche**

The design and synthesis of novel hybrid-silica nanoparticles (NPs) containing the FDA-approved antimicrobial triclosan (Irgasan) covalently linked within the inorganic matrix for its controlled, slow release upon interaction, is reported. The NPs are in the range of 130 ± 30 nm in diameter, with a smooth and spherical morphology. Characterization of the hybrid-silica NPs containing triclosan, namely T-SNPs, and their appropriate linkers is accomplished by microscopic and spectroscopic techniques. Preliminary antimicrobial activity is studied through bacterial-growth experiments. The T-SNPs are found to be superior in killing bacteria, as compared with the free biocide.

1. Introduction

In the context of increased bacterial resistance to common antibiotic treatments, nanoscale materials offer a unique opportunity to bring innovative and more-effective solutions to bacterial-disease control. Currently, several options have already been successfully explored using various types of organic/inorganic and composite nanomaterials. For example, such options include: i) silver (Ag) nanoparticles (NPs);[1] ii) carbon-based nanomaterials like single-walled carbon nanotubes (SWCNTs), C_{60} fullerenes, and graphene oxide;[1–4] iii) FDA-approved bioactive glasses (SiO_2–Na_2O–CaO–P_2O_5) of the 45S5 type;[1] iv) metal oxide (TiO_2, MgO, ZnO) NPs;[1,5] magnesium fluoride (MgF_2) NPs;[6] and v) chemically modified (antibiotic-decorated) gold (Au) NPs.[7] Each of these optional nanoscale systems clearly possesses its own specific mechanism of action, cellular target(s), potential delivery capability, and overall therapeutic advantages and disadvantages.

Inorganic-organic hybrid-silica nanoparticles (NPs), which are functionalized ceramic materials prepared from silicon dioxide, otherwise known as silica (SiO_2), have been employed as carrier systems for the controlled delivery of drugs, genes, and proteins.[8–10] The use of silica as a carrier system has received much attention because of its physical and chemical versatility (e.g., its ability to tune the mesoporous structure and control specific surface properties) and its nontoxic nature.[11,12] Indeed, compounds that can bridge inorganic and organic materials, such as silane-coupling agents bound to various functional moieties, are available. For example, silane-coupling agents can be used for surface grafting (via free silanol groups) of antibacterial agents. In order to increase the content of the deliverable molecules inside the inorganic matrix, one may incorporate a suitable silane derivative into the sol-gel synthetic process of the inorganic matrix in situ.[13] The modified Stöber method can be employed for this purpose.[14]

There are several ways to incorporate guest molecules into a sol-gel system. The first is the physical incorporation of drug substances, drug loading for example, into sol-gel-derived silica materials. This method was first introduced in 1983.[15] The sol-gel method is a simple, versatile and low-temperature way of preparing porous, amorphous ceramic materials that are light- and heat-stable without being hazardous to humans or to the environment.[16] Silica is an essential nutrient and plays an important role in many functions of living organisms, having a direct relationship to mineral absorption. Amorphous silica is nontoxic, biocompatible and biodegradable, freely dispersible throughout the body and ultimately excreted in the urine.[17] The feasibility of mesoporous silica as a drug-delivery system has been documented since the beginning of the millennium and has been subject to a number of reviews.[14,18–23] These studies have demonstrated that mesoporous silica can serve as a vehicle for the successful intracellular delivery of otherwise poorly soluble or membrane-impermeable agents.[24–26] The ceramic carrier matrix effectively protects the payload molecules from enzymatic degradation during delivery, as well as increases the solubility and permeability of a drug with otherwise poor bioavailability. Room-temperature-processed mesoporous silica is rapidly dispersed in water, but, when loaded with a large amount of guest molecules such as drugs, the aqueous solubility can be adversely affected due to the increased hydrophobicity of the pore walls.[17,27] The large adsorption (drug-loading) capacity is one of the many useful features of mesoporous silica materials, together with the control of material properties on the nanometer scale, such as the pore and particle sizes.[28]

An alternative to drug loading is covalently binding the guest molecules to the ceramic matrix. Although the reloading

I. Makarovsky, Dr. Y. Boguslavsky, M. Alesker, Prof. J.-P. Lellouche
Institute of Nanotechnology and Advanced Materials
Department of Chemistry
Bar-Ilan University
Ramat-Gan 52900, Israel
E-mail: Jean-Paul.M.Lellouche@biu.ac.il
J. Lellouche, Dr. E. Banin
The Mina and Everard Goodman Faculty of Life Science
Institute for Nanotechnology & Advanced Materials
Bar-Ilan University
Ramat-Gan 52900, Israel

DOI: 10.1002/adfm.201101557

property is thus lost in several cases, the greater stability, along with other advantages, such as controlled slow release, protection from degradation and modifiable solubility, are gained.

We have chosen this alternative as a model for our studies and triclosan (Irgasan) as the guest molecule to be incorporated inside the inorganic matrix. Triclosan is a well-known, commercial, Food and Drug Administration (FDA) approved, synthetic, non-ionic, broad-spectrum antimicrobial agent, possessing mostly antibacterial, but also some antifungal and antiviral properties.[29] Triclosan is fairly insoluble in aqueous solution, unless the pH is alkaline, and is readily soluble in most organic solvents. It is chemically stable and can be heated up to 200 °C for up to 2 h.[30] This thermal stability makes it suitable for incorporation into various reinforced plastic materials.

In 1998 the molecular target of triclosan was finally elucidated. Numerous studies conducted on different bacteria strains showed that triclosan acts on a defined bacterial target in the bacterial-fatty-acid biosynthetic pathway, the nicotinamide adenine dinucleotide (NADH)-dependent enoyl-[acyl carrier protein] reductase (ENR).[31–33] ENR catalyzes the final, regulatory step in the fatty-acid synthase cycle, the reduction of a carbon-carbon double bond in the enoyl moiety that is covalently linked to an acyl carrier protein. The phenol ring of triclosan forms a face-to-face interaction with the nicotinamide ring, allowing extensive π–π-stacking interactions. Additional Van der Waals contacts are made by both phenolic rings, with residues lining the active site, the substrate-binding pocket of the enzyme and the nucleotide cofactor. Hydrogen bonds are formed by the phenolic hydroxyl group of triclosan with the 2′–OH group of the nicotinamide ribose of the nucleotide and with the phenolic oxygen of tyrosine 156, which is believed to function as a proton donor during the catalytic cycle of ENR.[32,34]

Over the last 30 years, triclosan has become the most-potent and widely used bisphenol.[30] Triclosan is used in many contemporary consumer and professional health-care products. These include hand soaps, surgical scrubs, shower gels, deodorant soaps, health-care-personnel hand washes, hand lotions and creams, toothpastes, mouthwashes, and underarm deodorants.[29] Triclosan is also incorporated into fabrics and plastics, including children's toys, toothbrush handles, as well as surgical drapes, hospital over-the-bed table tops, etc. Triclosan has been extensively tested in humans and animals. Acute-toxicity, chronic-toxicity, mutagenicity, reproduction and teratology investigations have been recently reviewed.[29,35] Due to its poor bioavailability, triclosan-based products usually appear as formulations in various organic/inorganic matrix-loaded compounds.

Numerous papers have already been published on triclosan loading into an organic or inorganic matrix (e.g., melt-mixed into polystyrene for antibacterial efficacy, sustained-released from TiO_2 particles, inclusion into biodegradable β-cyclodextrin for bacteria-growth resistance, and loaded into poly(D,L-lactide-*co*-glycolide) (PLGA), poly(D,L-lactide) (PLA) and poly(vinyl alcohol) (PVAL) copolymers for periodontal disease, etc.).[36–45] Triclosan-loaded NPs (TiO_2 nanocapsules) have also been prepared, but triclosan has never been *covalently bound* to an inorganic matrix.[37] In this study we developed a linker that will allow covalent binding between silica NPs and triclosan. The covalent bond between the linker and the biocide is designed to be broken by enzymes, subsequently releasing the active triclosan, which will act upon its target inside the cell. Basically, the enzymes produced by the bacteria themselves will be responsible for the release of the antimicrobial agent. Such a covalent linkage ensures the above-mentioned properties and also prevents leaching, providing an improved mechanism for controlled release.

Herein, we report the design and synthesis of the innovative linker, triclosan-(3-(triethoxysilyl)propyl)carbamate (TTESPC), and the resulting nanosized, silica-based particles. Each particle contained the FDA-approved antibacterial agent, triclosan, covalently linked within the matrix for its controlled slow release upon interaction. The particles were prepared according to a modified Stöber method and the biocide-silanated linker was incorporated into the silica matrix during the particle-formation process. We demonstrate, that, for the first time (according to an extensive literature survey), a covalently bound biocide, namely triclosan, in an inorganic particulate matrix exerts its biological activity to the full extent and even exceeds that of the free biocide.

2. Results and Discussion

2.1. NPs Containing Covalently Bound Triclosan (T-SNPs)

The synthesis of triclosan-(3-(triethoxysilyl)propyl)carbamate (TTESPC) was accomplished through a direct carbamoylation of triclosan (**Figure 1**) with 3-isocyanatopropyltriethoxysilane in the presence of the Lewis acid, tetraoctyltin,[46] $Sn(Oct)_4$, as outlined in **Scheme 1**, and gave a yield of 64%. This is a new compound designed specifically to introduce the triclosan moiety inside the inorganic silica matrix. The relatively facile and efficient synthesis allows for an easy scale-up process.

It is a well-known fact that tin-based organometallic compounds catalyze reactions between hydroxyl compounds and isocyanates very efficiently.[47] The proposed structure of the TTESPC reagent was confirmed by ^{1}H-NMR, ^{13}C-NMR, IR, and UV–vis spectroscopy and mass spectrometry (MS) (Figure S1, Supporting Information). The presence of the aliphatic moieties upfield on the one hand (δ = 3.81, 3.20, 1.63, and 1.21 ppm) and the aromatic peaks slightly shifted downfield and more clustered indicate that covalent attachment had indeed occurred. The broad triplet at 5.3 ppm due to the proton attached to the carbamate nitrogen further confirmed that the reaction had succeeded (see the Experimental Section).

Once the TTESPC linker had been synthesized, the next step was to prepare the corresponding nanospheres with a desirable diameter of around 100–150 nm. We achieved this goal through a series of experiments using a modified Stöber method as

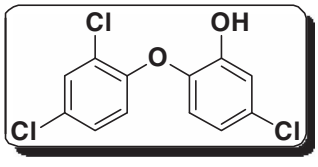

Figure 1. Chemical structure of triclosan (Irgasan).

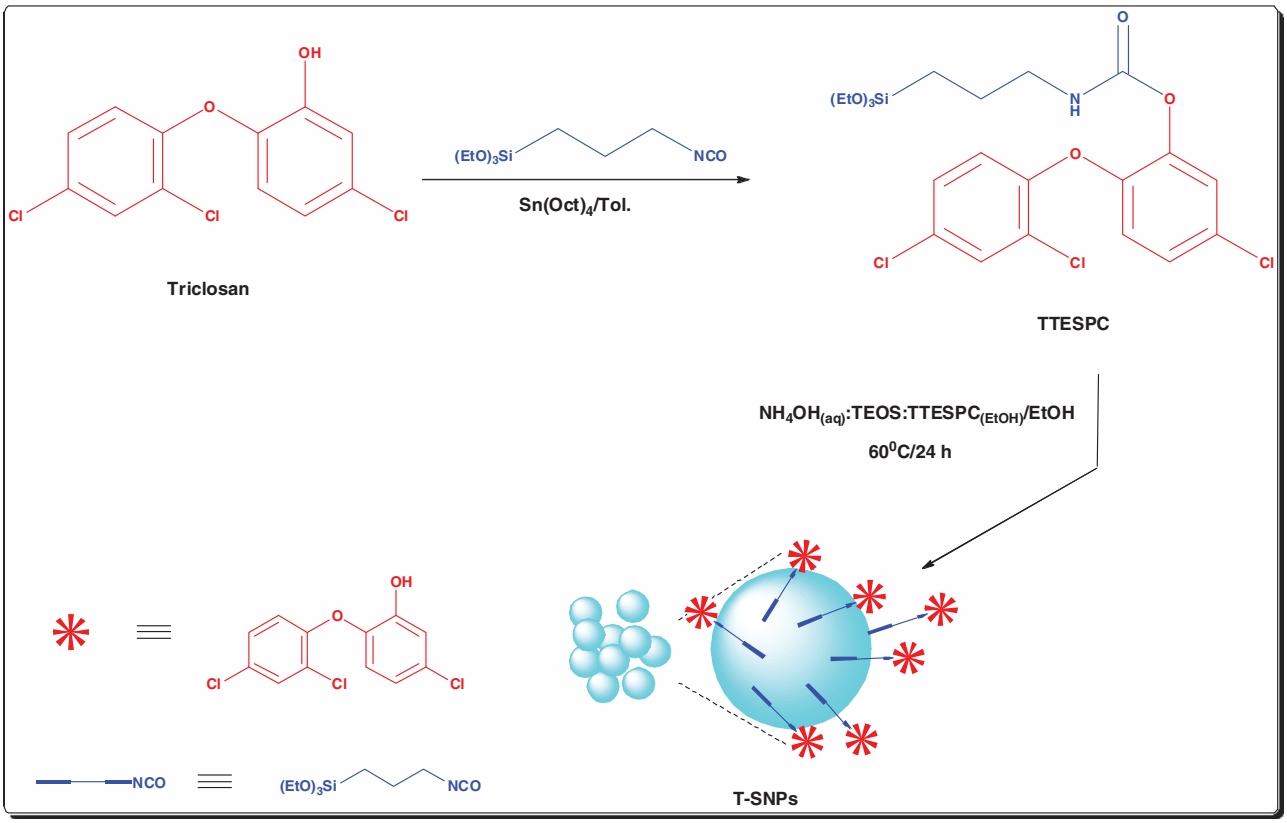

Scheme 1. A synthetic pathway for the fabrication of T-SNPs.

mentioned below. We found that a temperature dependence exists between the amount of linker added to the reaction mixture, the amount of linker found in the formed NPs and their subsequent relative diameters.

Figure 2A shows a correlation between the average nanoparticle diameter (measured by dynamic light scattering (DLS)) and the TTESPC's initial concentration. We observed that by reducing the linker's initial concentration from 10 to 2.5 wt%, the particle's diameter started stabilizing at a 200 nm value until reaching a final 160 nm one. The optimal compromise between the final triclosan weight percent inside the NPs and their corresponding diameter was obtained when an initial concentration of 2.5% (w/v) of the linker was added to the reaction mixture. In order to estimate the amount of linker present in the NPs, a measurable molecular entity could be used as an internal standard. For this purpose, measurable quantities of chlorine (Cl) could be directly correlated to the amount of incorporated triclosan: its quantity was determined by elemental analysis. Figure 2B describes the correlation between the initial linker concentration and the triclosan weight percentage inside the T-SNPs as a function of synthesis temperature. The dashed curve is for syntheses performed at 25 °C, for which no dependency of the triclosan content on the TTESPC concentration was observed. The solid curve relates to syntheses performed at 60 °C. One can observe that as the linker percentage diminishes and reaches a certain value, (2.5% w/w), the triclosan content inside the T-SNPs rises to 0.79 wt%. The amount of triclosan was calculated from the Cl quantity that was measured by elemental analysis (Equation 1). The rather-low final concentration of triclosan in the NPs was probably due to the relatively high hydrophobicity of the TTESPC, which hinders the incorporation of this sterically demanding linker into the midst of the inorganic, hydrophilic silica matrix.

Figure 3 shows scanning-electron-microscopy (SEM) and transmission-electron-microscopy (TEM) micrographs of the T-SNPs obtained in a typical experiment at 60 °C with 2.5% (w/v) of TTESPC. One can appreciate from these micrographs the smooth, spherical morphology of the NPs. These NPs were obtained with a narrow size distribution and an average diameter of 130 ± 30 nm. DLS studies showed a hydrodynamic diameter of 164.3 nm (Figure S2, Supporting Information), which is in a good accordance with the actual TEM size of similar dried particles, when considering the likely adsorption of water molecules onto the NP surface.

ζ-potential and particle-size titration versus rising pH was performed in order to estimate the relative stability of the NPs in aqueous media (Figure S3, Supporting Information). As one can observe, the ζ-potential increases in absolute value, from −8 mV at a pH of 3.7 to −36 mV at a pH of 12, which means that the particles became more stable. The ζ-potential is ≈−20 mV when the pH reaches a physiological value (pH = 7.4). Interestingly, the linker molecules, which are hydrophobic in nature, probably prefer to be oriented towards the inner part of the particle. Thus, the linker molecules have minimal influence on the net surface potential of the NPs. Further evidence of the stability of these particles is the lack

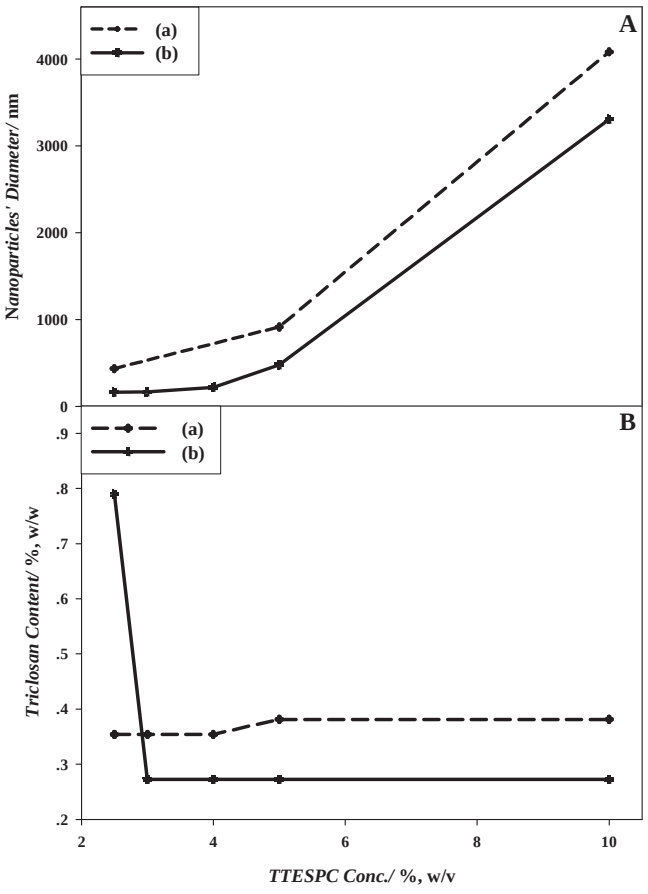

Figure 2. A) The effect of the initial TTESPC concentration on the average particle diameter, as measured by DLS, at 25 °C (dashed line, a) and 60 °C (solid line, b). B) The effect of the initial TTESPC concentration on the triclosan content, as calculated from elemental-analysis data (dashed line, a: 25 °C; solid line, b: 60 °C).

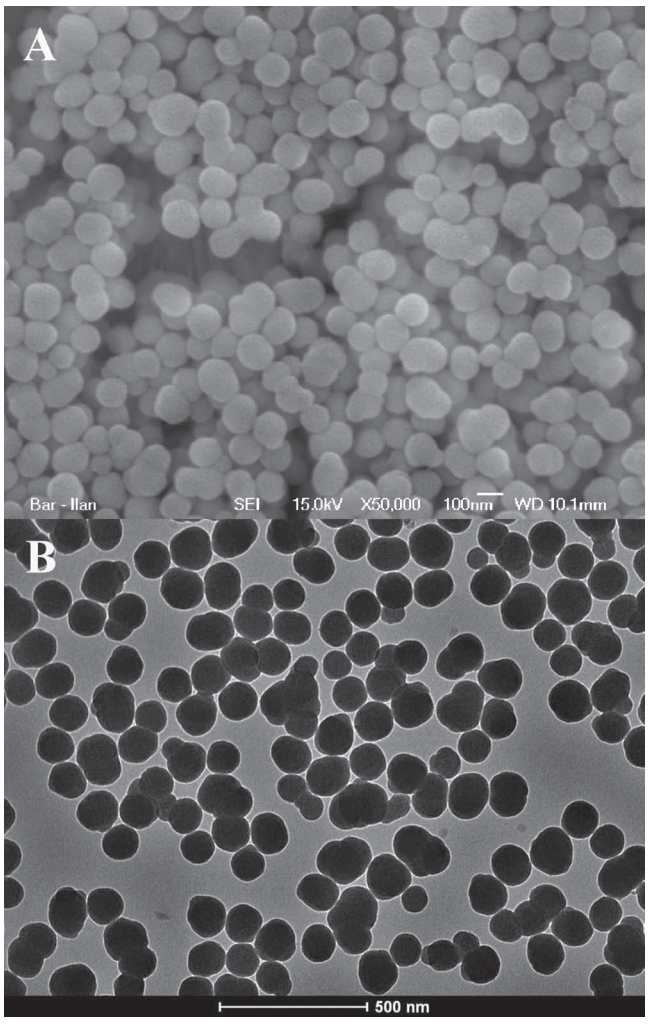

Figure 3. A) HR-SEM micrograph of T-SNPs (scale: 100 nm). B) TEM (scale: 500 nm) micrograph of T-SNPs.

of aggregation over a relatively wide pH-value range, since the measured average diameters of the T-SNPs remain practically stable until a pH of 10, disclosing 150–170 nm values (i.e., very close to their TEM-measured diameter).

Figure 4 shows the Fourier transform IR (FTIR) spectra of the linker, TTESPC, and the T-SNPs and reveals the characteristic peaks of the functional groups present. The IR spectrum of TTESPC (Figure 4a) reveals absorption peaks at 3320 cm^{-1}, which corresponds to the carbamate NH asymmetric-stretching band, 2885–2974 cm^{-1} (alkane CH_2 asymmetric stretching bands), 1717 cm^{-1} (carbamate C=O stretching band), 1487 cm^{-1} (aromatic C=C stretching bands), 1280 cm^{-1} (Si–O–C stretching bands), 1080 cm^{-1} (phenolic symmetrical C–O stretching bands), and 789 cm^{-1} (C–Cl stretching bands). The IR spectrum of the T-SNPs (Figure 4b) shows a broad curve with a peak at 3390 cm^{-1}, which corresponds to the carbamate NH and alkane CH_2 asymmetric-stretching bands, a peak at 1639 cm^{-1} (a red-shifted carbamate C=O stretching band), a broad curve with a peak at 1108 cm^{-1} (Si–O–C ether stretching bands, aromatic C=C stretching bands and phenolic symmetrical C–O stretching bands), a peak at 949 cm^{-1} (aromatic C–H stretching bands), and a peak at 789 cm^{-1} (C–Cl stretching bands). A wavenumber shift of the CO stretching ($\nu_{C=O}$) band gives insight into the molecular interaction occurring in the system under study. In particular, the shift to lower wavenumbers ("red-shift") may be attributed to the presence of hydrogen-bond interactions with the carbamate carbonyl inside the inorganic solid SiO_2 matrix. The opposite effect, namely the shift to higher wavenumbers, ("blue-shift") of the ν_{CH} band of alcohols in polar organic compounds and surfactants observed for aqueous solutions, has also been observed.[48]

Figure 5 illustrates the thermal analyses performed on the T-SNPs. Curve a corresponds to the thermogravimetric-analysis (TGA) thermogram (using a 25–500 °C temperature profile; 10 °C min^{-1}, N_2 atmosphere, 100 mL min^{-1}). This thermogram consists of several slopes, with one main-step slope showing approximately 3% weight loss (at approximately 100 °C), which may correspond to a loss of water molecules entrapped in the inorganic matrix. The second slope, between approximately 100 and 190 °C (approximately 2% weight loss) may correspond to a loss of the water molecules that participate in the hydrogen bonding between the silanol groups on the surface and near the surface[49] and a release of CO gas from the NPs as their

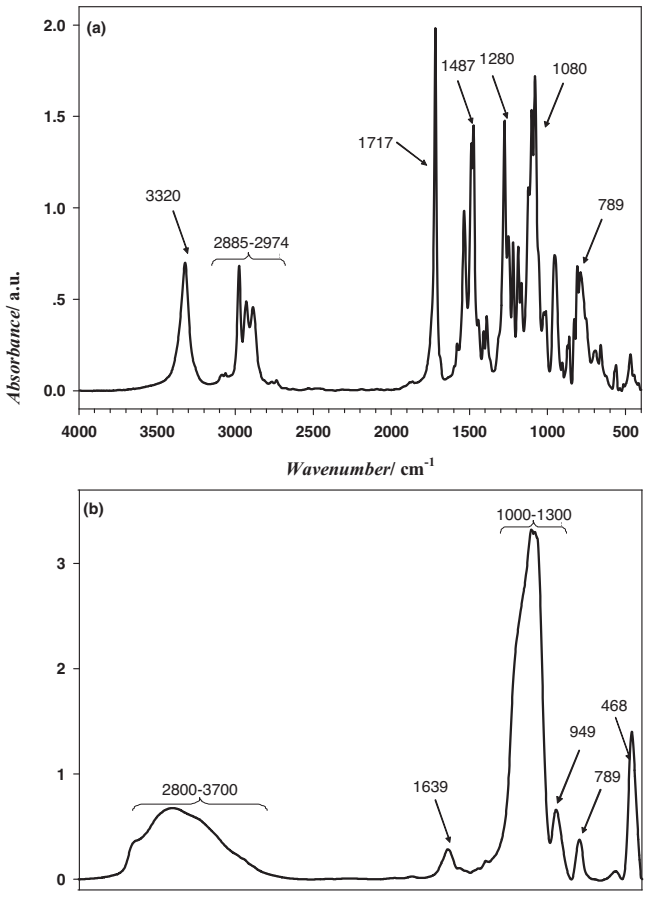

Figure 4. a) FTIR spectrum of the linker, TTESPC. b) FTIR spectrum of the T-SNPs.

degradation starts. This fact may be corroborated with the DSC thermogram (see the long-dashed curve d, Figure 5), with two proximal exothermic peaks between 110 and 200 °C. Afterwards, the degradation of the organic content begins, as evidenced by the moderate weight loss in the TGA curve (approximately 6.5% weight loss) and the moderate exotherm in the DSC thermogram.

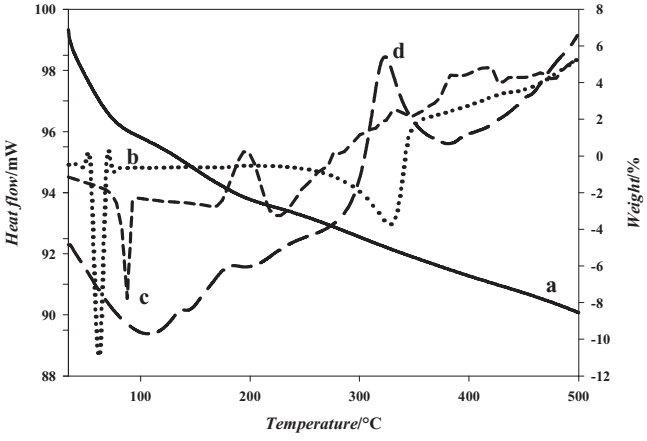

Figure 5. TGA thermogram of T-SNPs (curve a) and DSC thermograms of triclosan (curve b), TTEPSC (curve c), and T-SNPs (curve d).

The exotherm with its peak at 320 °C may be attributed to the formation of radicals created as a result of chlorine-radical combination into Cl_2. The same peak appears in the DSC thermogram of the linker itself but shifted to a much lower temperature (approximately 190 °C). This can be explained by the fact that the inorganic matrix shields and protects the entrapped linker molecules from the external environment, resulting in a higher degradation temperature. Curves b (dotted curve) and c (short-dashed curve) correspond to DSC thermograms of triclosan and of the linker, TTESPC, respectively. One can clearly see one sharp endotherm in each curve, with peaks corresponding to the melting points of triclosan and TTESPC (i.e., 56 °C and 83 °C in curves b and c respectively). There is another endotherm, at approximately 344 °C, corresponding to the boiling point of triclosan. Beyond this point, the NP decomposition begins. The lack of the peaks mentioned before in curve d further emphasizes the covalent attachment of the linker to the inorganic matrix, as well as the absence of the free biocide or linker within the inorganic matrix of the T-SNPs.

2.2. Preliminary Biological Results

In order to investigate the antimicrobial activity of these NPs, a series of biological experiments were designed and carried out. **Figure 6** depicts the antimicrobial activity of the T-SNPs against two common bacterial pathogens, *Escherichia coli* (E. coli) (Gram-negative) and *Staphylococcus aureus* (S. Aureus) (Gram-positive), in the presence of different concentrations of T-SNPs. The results presented demonstrate that, for the two types of bacteria, the T-SNPs caused a reduction in growth in a dose-dependent manner and the minimal bactericidal concentration (MBC) measured was 10 μg mL^{-1} for both *E. coli* and *S. aureus*. Despite the similar MBCs, we observed a difference in the sensitivity of these strains to the T-SNPs treatment. *E. coli* seems to be more sensitive compared with *S. aureus*, and complete killing was observed after 14 h, whereas complete killing of *S. aureus* was observed only after 22 h. Unloaded SNPs, and TTESPC (the linker itself) served as controls and no antibacterial activities were observed.

Next, we wanted to rule out the possibility of the leaching of triclosan from the NPs (even without the presence of bacteria), which would suggest that the T-SNPs are unstable. A high concentration of T-SNPs (50 μg mL^{-1}) was incubated in a growth medium (without bacteria) for 24 h (same conditions as for the killing experiments mentioned below). Then, the NPs were centrifuged, filtered and the supernatant was incubated separately with *E. coli* and *S. aureus* and their growth was monitored. It can clearly be observed from the plotted graphs (Figure 6A,B, dashed curves) that the growth rates of the two pathogens were not impeded and resembled the control. This strongly suggests that the activity required the presence of bacteria and that either no triclosan was released from the T-SNPs in the first incubation step or the amount of released triclosan remained very low and was not sufficient to impede bacterial growth. To further validate that the antimicrobial properties of the T-SNPs were solely mediated by the release of triclosan, a second series of experiments was done. In this experiment, we grew a triclosan-resistant *E. coli* RJH108 strain with the highest tested

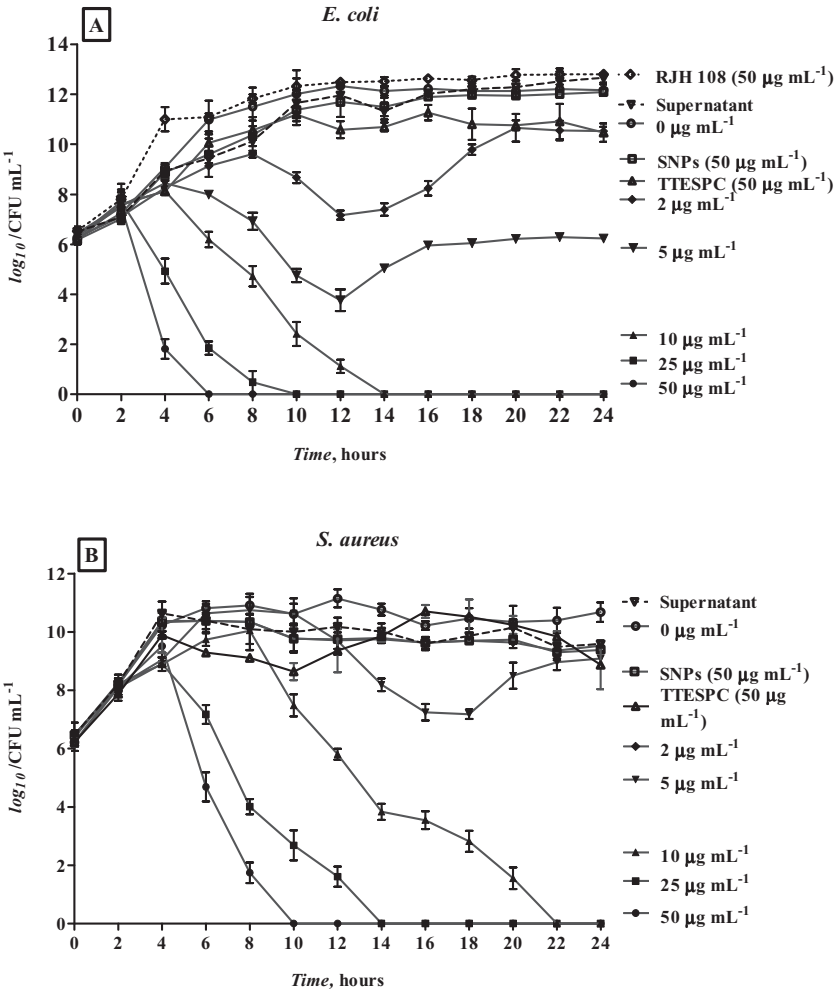

Figure 6. A–B) Antimicrobial activity of T-SNPs. Killing curves of *E. coli* (A) and *S. aureus* (B) grown in different concentrations of T-SNPs (2 to 50 μg mL^{-1}) are shown. The growth was determined by the viable counts and is expressed in colony-forming units (CFU). *E. coli* RJH108 (dotted-curve line in A) represents the growth of the triclosan-resistant strain exposed to the T-SNPs at a concentration of 50 μg mL^{-1}. The dashed-curve lines refer to *E. coli* (A) and *S. aureus* (B) grown in the supernatant of TSB or TSB-Glu previously incubated with T-SNPs (50 μg mL^{-1}) for 24 h at 37 °C. Untreated bacteria and unloaded NPs (SNPs 50 μg mL^{-1}) served as positive and negative controls respectively. The error bars represent the standard deviation of *three* independent experiments.

concentration of T-SNPs (50 μg mL^{-1}).[33] We reasoned that if the triclosan does indeed induce the killing of the bacteria, this strain, being resistant to triclosan, will survive. Indeed, this strain was not affected by the presence of the T-SNPs (dotted line in Figure 6a).

Our next step was to compare our T-SNPs with regard to the activity of free triclosan. The MBC of the *free* triclosan that affected the growth of the two types of bacteria was measured (**Figure 7**A,B) and found to be 0.1 μg mL^{-1}. This result is in accordance with known literature data.[50,51] A similar killing-curve pattern was observed with the T-SNPs, yet with a significant distinction. As calculated from the elemental analysis, the triclosan constituted only 0.79 wt% of the NPs, meaning that the highest concentration of NPs taken for the experiments, 50 μg mL^{-1}, encompassed only 0.041 μg mL^{-1} of *covalently bound* triclosan. At this concentration, the *free* triclosan only began to impede the bacterial growth, whereas *the T-SNPs killed all of the bacteria*. At this concentration of triclosan (≈0.04 μg mL^{-1}, dotted lines in Figure 7a,b), the T-SNPs afforded an increase of 5–6 log in killing capacity compared with the *free* biocide. It is likely that the strong antimicrobial effect stems from the protection of the harsh chemical and/or biochemical environment provided by the NPs during delivery. For example, silica matrices are known to provide UV protection.[52–54] This means that these matrices prevent the UV-sensitive triclosan from UV-induced decomposition to deleterious dioxins.[55] Furthermore, the T-SNPs may deliver a local high concentration of triclosan near the bacteria via membrane attachment, thus increasing its overall efficacy.

To examine the possibility that the T-SNPs intimately interact with the bacteria, TEM measurements were conducted to investigate the mode of action of the NPs on the tested cells (**Figure 8**). Untreated *E. coli* and *S. aureus* (Figure 8A,B) cells both showed the normal cell morphology, possessing the distinct cell walls and membrane structures typical of Gram-negative and Gram-positive bacteria. Quite interestingly, the T-SNP-treated samples of both *E. coli* and *S. aureus* (Figure 8C,D) showed that the interacting T-SNPs were localized either on the cell surface or within the cell membrane, disclosing pronounced damage to the cell walls (Figure 8E,F). Although no NP internalization was detected, our imaging results reinforce the importance of *direct* NP-bacteria interactions for the promoted antibacterial activity. In this manner, TEM analyses further direct us to a possible mechanism of action of the T-SNPs, emphasizing the importance of the role played by membrane-associated enzymes in the triclosan-release phase. The presence of enzymes in general and esterases in particular is known in the literature.[56]

3. Conclusions

We have designed, synthesized, and fully characterized a novel and potentially multifunctional nanosized particulate SiO_2 matrix that, upon enzymatic degradation (esterases), can release the FDA-approved antimicrobial agent, triclosan, in a controlled manner. Triclosan is covalently linked inside the hybrid-SiO_2 NPs that are thus intrinsically designed to withhold the release of the biocide without any prior direct interaction with pathogenic bacteria. Preliminary biological experiments dealing with these T-SNPs show an unexpected and remarkably enhanced

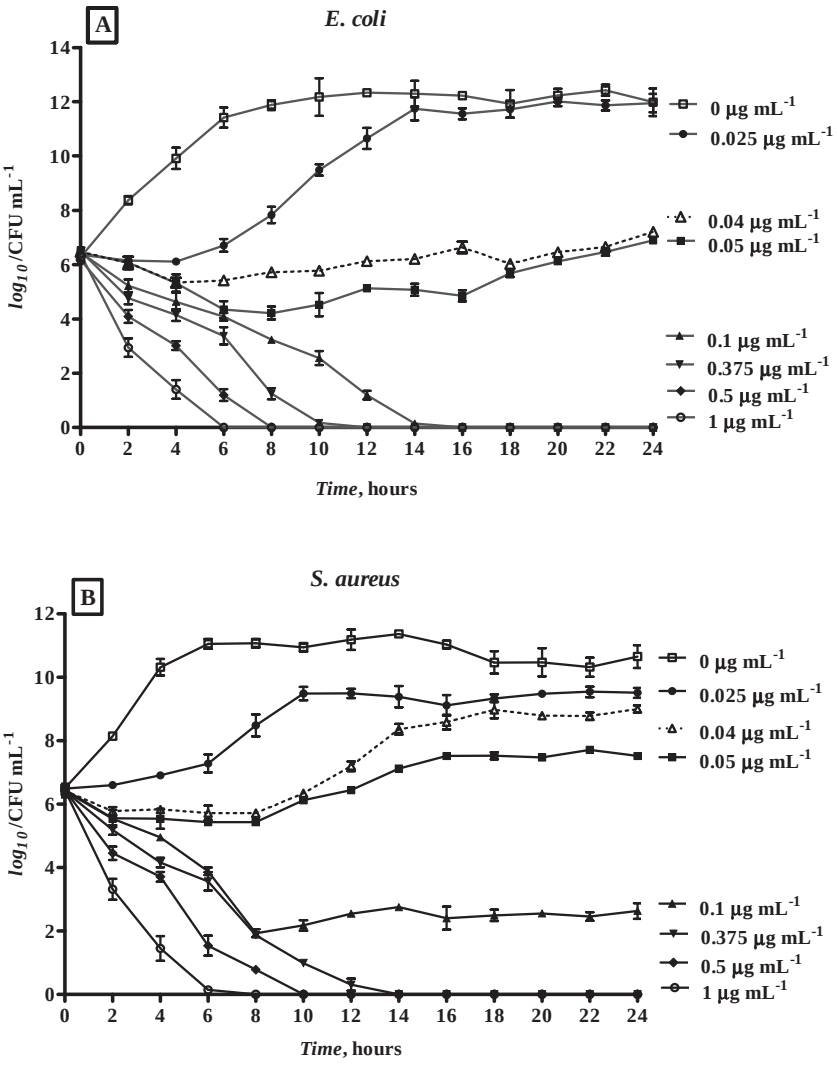

Figure 7. A–B) Minimal inhibitory concentration (MIC) of triclosan. Killing curves of *E. coli* (A) and *S. aureus* (B) exposed to variable concentrations of free-triclosan (0.025 to 1 μg mL^{-1}) solutions. Untreated bacteria served as a negative control. The error bars represent the standard deviation of *three* independent experiments. The dotted 0.04 μg mL^{-1} killing curves correspond to the effective T-SNPs concentration mentioned in Figure 6.

antimicrobial activity (an increase of 5–6 log in killing capacity compared to the *free* biocide). This is probably due to the controlled, contact-mediated delivery of the antimicrobial particles, each serving as a lethal "Trojan horse" during the NP digestion/bioenzymatic degradation (patent design/material),[57] where the triclosan molecule is presumably released.

Further biological studies are currently being undertaken that will enable us to get a deeper insight into the overall mechanism of the biocidal action of these NPs in order to enhance and control their efficacy even more.

4. Experimental Section

Chemicals and Reagents: The following analytical-grade chemicals were purchased from Aldrich and were used without further purification: triclosan (Irgasan) (>97%), ethanol (EtOH) (high-performance liquid chromatography (HPLC) grade), toluene (99.8%), 3-(triethoxysilyl)propyl isocyanate (95%), ammonium hydroxide (A.C.S. reagent grade), and tetraethyl orthosilicate (TEOS) (99.999%). Tetraoctyltin (for synthesis) was purchased from Merck. Water was purified by the passage of deionized water through an Elgastat Spectrum reverse-osmosis system (Elga Ltd., High Wycombe, UK).

Triclosan-(3-(triethoxysilyl)propyl)carbamate (TTESPC): Triclosan (5-chloro-2-(2,4-dichlorophenoxy)phenol) (1 g, 3.45 mmol, 1 eq) and dry toluene (5.0 mL) were added to a three-necked round-bottom flask under a N_2 atmosphere, so as to obtain a 0.7 M solution. 3-(Triethoxysilyl) propyl isocyanate (1.28 mL, 5.18 mmol, 1.5 eq) and tetraoctyltin (3.02 mL, 5.18 mmol, 1.5 eq) were added simultaneously to the reaction mixture, which was stirred at room temperature until no progress in the reaction could be observed by thin-layer chromatography (TLC) (4:1 n-hexane:EtOAc) n-hexane:ethyl acetate (EtOAc)). Toluene was evaporated until an off-white oil emerged. Upon crystallization overnight, white crystals were obtained. These were filtered with cold n-hexane to remove traces of the stannane complex and dried under vacuum to yield 63.5% (1.17 g) of a white crystalline powder. mp 83–84 °C; ^{1}H NMR (300 MHz, $CDCl_3$, 25 °C, TMS, δ): 7.43 (d, J = 2.5 Hz, 1H, ClCC***H***Cl), 7.26 (d, J = 2.5 Hz, 1H, ClCC***H***C(O)C(O)), 7.15 (dd, J = 8.8, 2.5 Hz, 1H, ClCC***H***CHC(O)CCl), 7.13 (d, J = 2.5 Hz, 1H, ClCC***H***CHC(O)C(O)), 6.87 (d, J = 8.8 Hz, 1H, ClCCHC***H***C(O)C(O)), 6.83 (d, J = 8.8 Hz, 1H, ClCCHC***H***C(O)CCl), 5.36 (bt, 1H, N***H***), 3.81 (q, J = 7.0 Hz, 6H, $CH_3C\boldsymbol{H}_2O$), 3.20 (m, 2H, $NHC\boldsymbol{H}_2$), 1.63 (m, 2H, $NHCH_2C\boldsymbol{H}_2$), 1.21 (t, J = 7.0 Hz, 9H, $C\boldsymbol{H}_3CH_2O$), 0.62 (m, 2H, $SiC\boldsymbol{H}_2$); ^{13}C NMR (75.5 MHz, $CDCl_3$, 25 °C, TMS, δ): 153.2 (1C, NH***C***=O(O)), 151.4 (1C, CH***C***(O)C(O)), 147.0 (1C, Cl***C***(O)CH), 142.3 (1C, $NHCO_2\boldsymbol{C}$), 130.2 (1C, ClC***C***HCl), 129.3 (1C, Cl***C***CHC(O)), 129.1 (1C, Cl***C***CHCHC(O)CCl), 128.1 (1C, ClC***C***HCHC(O)CCl), 126.4 (1C, ClC***C***HCHC(O)C(O)), 125.6 (1C, Cl***C***C(O)CH), 124.8 (1C, ClC***C***HC(O)), 120.4 (1C, ClCCH***C***HC(O)CCl), 120.2 (1C, ClCCH***C***HC(O)C(O)), 58.5 (3C, $CH_3\boldsymbol{C}H_2O$), 43.6 (1C, $NH\boldsymbol{C}H_2$), 22.8 (1C, $NHCH_2\boldsymbol{C}H_2$), 18.2 (3C, $\boldsymbol{C}H_3CH_2O$), 7.5 (1C, $Si\boldsymbol{C}H_2$); IR (KBr): ν = 3320 (m; ν_{as}(NH)), 2974 (m; $\nu_{as}(CH_2)$), 2927 (m; $\nu_{as}(CH_2)$), 2885 (m; $\nu_{as}(CH_2)$), 1717 (vs; ν(C=O)), 1534 (s), 1487 (s; ν_{as}(aromatic C=C)), 1474 (vs), 1389 (w), 1280 (vs; ν_{as}(SiOC)), 1250 (m), 1219 (m), 1187 (m), 1080 (vs; ν_s(phenolic CO)), 956 (m; ν_{as}(aromatic CH)), 789 cm^{-1} (m; ν_{as}(CCl)); UV–vis (EtOH): λ_{max} (ε) = 276 (2822), 230 (17 407), 209 nm (32 160); CIMS (m/z (%)) 536.08 (M^+, 5.48), 489.98 ($C_{20}H_{23}Cl_3NO_5Si^{\bullet}$, 100.00); HRMS (ESI, m/z): $[M + H]^+$ calcd for $C_{22}H_{28}Cl_3NO_6Si$, 535.905; found, 536.085.

Hybrid-Silica NPs Containing Triclosan (T-SNPs): General Procedure Using a Modified Stöber Method: 2.4 mL of a 28–30% solution of aqueous NH_4OH and 25 mL of HPLC grade absolute ethanol were added to a 100 mL vial containing a stirrer at a certain temperature (25 or 60 °C, depending on the experiment). The medium was stirred for 5 min to obtain a homogeneous clear solution. Meanwhile, TTESPC (72.1 mg, 2.5% n/n) was dissolved completely in an additional 5 mL of ethanol and added to the previously described solution. The mixture was stirred for an additional 15 min in order to hydrolyze the silicate groups of the linker (TTESPC). Finally, 1.2 mL of TEOS were added to the clear solution, which was then stirred for 24 h at ambient temperature. T-SNPs of various

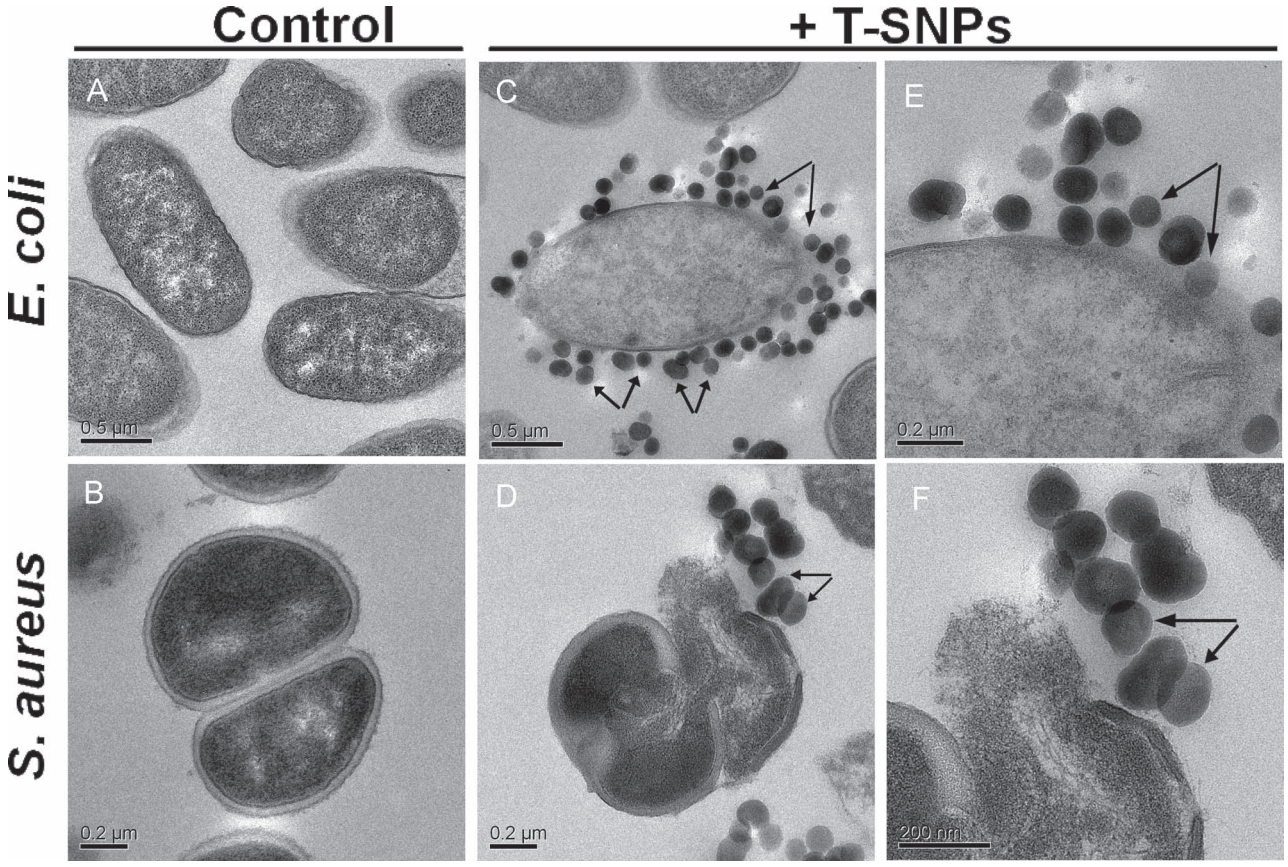

Figure 8. A–F) TEM of T-SNPs-treated and untreated cells. TEM micrographs of *E. coli* and *S. aureus* thin sections: untreated *E. coli* (A) and untreated *S. aureus* (B); *E. coli* exposed to T-SNPs (50 µg mL^{-1}) after 2 h (C) and *S. aureus* exposed to T-SNPs after 4 h of treatment (D). E–F) Magnified images of the adjacent micrographs (C and D). The arrows indicate the presence of T-SNPs.

sizes, size distributions and stabilities were prepared by changing the sol-gel process parameters (e.g., linker, base and TEOS concentrations), as well as the medium temperature. The resulting NPs were washed with EtOH using sequential centrifugation cycles (13 000 rpm) until a neutral pH was reached, then were washed twice with H_2O. Finally, the NPs were lyophilized to dryness.

Analytical Methods and Instrumentation: ^{1}H- and ^{13}C-NMR spectra were obtained using a Bruker DPX 300 MHz spectrometer. The chemical shifts are expressed in ppm downfield from Me_4Si (tetramethylsilane (TMS)) used as an internal standard. The values are given using the δ scale. Multiplicities in the ^{13}C-NMR spectra were determined by off-resonance decoupling. All of the moisture-sensitive reactions were carried out in flame-dried reactions vessels. The melting points were determined using an electrothermal digital melting-point apparatus. The progress of the reactions was monitored by TLC.

Mass spectra (MS) and high-resolution mass spectra (HRMS) were obtained using a MICROMASS-AutoSpec high-resolution magnetic-sector mass spectrometer connected to an HP-5890 series II gas chromatograph (Cl^+, chemical ionization).

High-resolution-SEM and energy-dispersive-spectroscopy (EDS) analyses were carried out on a JEOL JSM-7000F instrument. TEM and HR-SEM analyses enabled the determination of the morphology, size and size distribution of the particles, while EDS and elemental analyses provided particle-composition data. The TEM micrographs were taken using a Tecnai Spirit instrument (120 kV). Samples for TEM were prepared by placing a drop of the diluted spheres dispersed in an (50% v/v) ethanol-water solution on 400 mesh carbon-covered Cu grids Pk/100 (SPI Supplies West Chester, USA) and then air-drying them. The average diameter, particle-size distribution, and surface morphology of the particles were obtained by SEM or TEM, followed by a statistical analysis (ImageJ software) by measuring at least 200 particles for each sample. The SEM samples were coated with a thin layer of gold by a sputtering deposition technique.

Thermal measurements were performed by TGA and DSC. The TGA measurements were carried out using a TA Instruments apparatus (1GA Q500 model) for TGA, and DSC using a METTLER TOLEDO DSC 822^e instrument, with a 25–500 °C temperature profile (10 °C min^{-1}, N_2 atmosphere, 100 mL min^{-1}) for both. TGA afforded the temperature profiles of the hybrid-silica particles versus TTESPC. DSC revealed the endothermic and exothermic processes involving the hybrid-silica particles versus the linker during the heating process.

Elemental (chlorine) analysis of the NPs was performed using a combination of an oxygen-flask combustion technique and subsequent ion chromatography (DIONEX). The relative quantity of triclosan was calculated according to Equation 1:

$$\frac{mol_f(\mathrm{Cl})}{3} \times 289.64 \ \frac{\mathrm{g}}{\mathrm{mol}} \ (M_w \text{ of triclosan}) = \%\ \text{triclosan inside the T} - \text{SNPs} \quad (1)$$

In Equation 1, mol_f indicates the amount of chlorine in moles found by elemental analysis. The expression is divided by 3 due to the presence of 3 chlorine atoms in the triclosan molecule. If one assumes that the amount of chlorine found relates to an arbitrary 100 mass units, the expression result indicates percentages.

The hydrodynamic particle size, size distribution and ζ-potential of the particles were determined using a Zetasizer Nano series instrument (Nano-ZS, Malvern Instruments Ltd., UK) equipped with an MPT-2 multi-purpose titrator (Malvern Instruments Ltd., UK). ζ-Potential titration analyses were used in order to follow-up the colloidal stability of the hybrid-silica NPs towards aggregation.

FTIR-spectroscopy analysis was performed using a Brüker Equinox 55 FTIR spectrometer. The analysis was performed using 13 mm-diameter KBr pellets that contained 2 mg of the sample and 198 mg of KBr. The pellets were subjected to 200 scans at a resolution of 4 cm^{-1}.

A UV-spectrophotometer (CARY 100 Bio UV–vis spectrophotometer) was utilized to further characterize the TTESPC and the resulting T-SNPs (due to the presence of the UV-active chromophore).

Bacterial Cultures and Growth Conditions: *E. coli* and *S. aureus* 8325 were grown in Tryptic Soy Broth (TSB) (Difco) and Tryptic Soy Broth 66% supplemented with glucose (0.2%) (TSB-Glu) media, respectively, at 37 °C.

Leaching Test: To exclude the possibility of the presence of non-covalently linked triclosan in concentrations below the detection limits of UV spectroscopy, we exposed *E. coli* and *S. aureus* in media previously incubated for 24 h at 37 °C with T-SNPs at a high concentration of 50 μg mL^{-1}. Before medium addition, the T-SNPs were removed by centrifuging the TSB or TSB-Glu medium for 20 min at 14 000 rpm. Stationary phase bacteria in TSB or TSB-Glu were diluted to 10 mL to produce the desired starting inocula of 10^6 CFU mL^{-1} of medium. Samples (100 μL) were removed from each well every 2 h and serial dilutions were plated on Luria–Bertani agar to determine the CFU.

Killing-Curve Assay: Killing curves were determined in triplicate using starting inocula of 10^6 CFU mL^{-1}. Fresh, overnight growths of bacteria in TSB or TSB-Glu were diluted as necessary to produce the desired starting inocula in 10 mL of medium. T-SNPs and triclosan were tested in concentration ranges from 0 to 50 μg mL^{-1} and 0 to 1 μg mL^{-1} respectively. Silica nanoparticles (SNPs) were added at the highest tested concentration (50 μg mL^{-1}). TTESPC was previously dissolved in dimethyl sulfoxide (DMSO) and added to the media at a concentration of 50 μg mL^{-1}. Samples (100 μL) were removed from each well every 2 h and diluted appropriately in saline. Colony-forming units were determined by spotting 5 μL samples in triplicate on Luria–Bertani agar plates after 24 h incubation at 37 °C. To confirm that the antimicrobial properties of the T-SNPs were mediated by the sole release of triclosan, the triclosan-resistant strain of *E. coli*, RJH108, was exposed to the highest concentration of T-SNPs tested (50 μg mL^{-1}).[33] The viability was determined by using the same experimental protocol as described above.

TEM of Bacterial Samples: Samples of the *E. coli* and *S. aureus* cultures were centrifuged and washed immediately after 2 or 4 h (for *E. coli* and *S. aureus*, respectively) of treatment with and without T-SNPs (50 μg mL^{-1}). The samples were then fixed in 25% pentane-1,5-dial/polyoxymethylene in a cacodilate buffer at room temperature for 1 h. Then, the samples were washed with the same cacodilate buffer and fixed in 1% osmium tetraoxide (OsO_4). Sample embedding was carried out using a standard protocol (polymerized beads of agar resin) and 60 nm-thick slices were cut with a diamond knife (LBR ultratome III).[58] The resulting slices were deposited on bare 200 mesh copper grids, and stained with 2 wt% uranyl acetate for 5 min. Finally, the grids were dried in a desiccator and examined using a Fei Tecnai g2 instrument at 120 kV.

Supporting Information

Supporting Information is available from the Wiley Online Library or from the author.

Acknowledgements

Financial support of this work from the Israeli Ministry of Industry (Biofouling Magnet program) is gratefully acknowledged.

Received: July 10, 2011
Published online: September 13, 2011

[1] L. Matthews, R. K. Kanwar, S. Zhou, V. Punj, J. R. Kanwar, *Open Tropical Med. J.* **2010**, *3*, 1.
[2] A. Niu, Y. Han, J. Wu, N. Yu, Q. Xu, *J. Phys. Chem. C* **2010**, *114*, 12728.
[3] O. Akhavan, E. Ghaderi, *ACS Nano* **2010**, *4*, 5731.
[4] W. Hu, C. Peng, W. Luo, M. Lv, X. Li, D. Li, Q. Huang, C. Fan, *ACS Nano* **2010**, *4*, 4317.
[5] P. Hajkova, P. Spatenka, J. Horsky, I. Horska, A. Kolouch, *Plasma Processes Polym.* **2007**, *4*, S397.
[6] J. Lellouche, E. Kahana, S. Elias, A. Gedanken, E. Banin, *Biomaterials* **2009**, *30*, 5969.
[7] S. A. Kumar, Y.-T. Chang, S.-F. Wang, H.-C. Lu, *J. Phys. Chem. Solids* **2010**, *71*, 1484.
[8] C. Y. Lai, B. G. Trewyn, D. M. Jeftinija, K. Jeftinija, S. Xu, S. Jeftinija, V. S. Y. Lin, *J. Am. Chem. Soc.* **2003**, *125*, 4451.
[9] B. Munoz, A. Ramila, J. Perez-Pariente, I. Diaz, M. Vallet- Regi, *Chem. Mater.* **2002**, *15*, 500.
[10] J. Jang, Y. Kim, *Chem. Commun.* **2008**, 4016.
[11] C. Kneuer, M. Sameti, E. G. Haltner, T. Schiestel, H. Schirra, H. Schmidt, C.-M. Lehr, *Int. J. Pharm.* **2000**, *196*, 257.
[12] A. Sayari, S. Hamoudi, *Chem. Mater.* **2001**, *13*, 3151.
[13] L. L. Hench, J. K. West, *Chem. Rev.* **1990**, *90*, 33.
[14] I. I. Slowing, J. L. Vivero-Escoto, C.-W. Wu, V. S. Y. Lin, *Adv. Drug Delivery Rev.* **2008**, *60*, 1278.
[15] K. Unger, H. Rupprecht, B. Valentin, W. Kircher, *Drug Dev. Ind. Pharm.* **1983**, *9*, 69.
[16] H. Böttcher, P. Slowik, W. Süß, *J. Sol-Gel Sci. Technol.* **1998**, *13*, 277.
[17] J. Andersson, J. Rosenholm, S. Areva, M. Lindén, *Chem. Mater.* **2004**, *16*, 4160.
[18] S. Cosnier, S. Szunerits, R. S. Marks, J. P. Lellouche, K. Perie, *J. Biochem. Biophys. Methods* **2001**, *50*, 65.
[19] M. Hartmann, *Chem. Mater.* **2005**, *17*, 4577.
[20] M. Vallet-Regí, F. Balas, D. Arcos, *Angew. Chem. Int. Ed.* **2007**, *46*, 7548.
[21] B. G. Trewyn, S. Giri, I. I. Slowing, V. S.-Y. Lin, *Chem. Commun.* **2007**, 3236.
[22] S. Giri, B. G. Trewyn, V. S.-Y. Lin, *Nanomedicine* **2007**, *2*, 99.
[23] I. I. Slowing, B. G. Trewyn, S. Giri, V. S.-Y. Lin, *Adv. Funct. Mater.* **2007**, *17*, 1225.
[24] J. Lu, M. Liong, J. I. Zink, F. Tamanoi, *Small* **2007**, *3*, 1341.
[25] M. Liong, J. Lu, M. Kovochich, T. Xia, S. G. Ruehm, A. E. Nel, F. Tamanoi, J. I. Zink, *ACS Nano* **2008**, *2*, 889.
[26] I. I. Slowing, B. G. Trewyn, V. S.-Y. Lin, *J. Am. Chem. Soc.* **2007**, *129*, 8845.
[27] A. Galarneau, M. Nader, F. Guenneau, F. Di Renzo, A. Gedeon, *J. Phys. Chem. C* **2007**, *111*, 8268.
[28] J. M. Rosenholm, A. Meinander, E. Peuhu, R. Niemi, J. E. Eriksson, C. Sahlgren, M. Lindén, *ACS Nano* **2008**, *3*, 197.
[29] R. D. Jones, H. B. Jampani, J. L. Newman, A. S. Lee, *Am. J. Infection Control* **2000**, *28*, 184.
[30] H. N. Bhargava, P. A. Leonard, *Am. J. Infection Control* **1996**, *24*, 209.

[31] L. M. McMurry, M. Oethinger, S. B. Levy, *Nature* **1998**, *394*, 531.
[32] C. W. Levy, A. Roujeinikova, S. Sedelnikova, P. J. Baker, A. R. Stuitje, A. R. Slabas, D. W. Rice, J. B. Rafferty, *Nature* **1999**, *398*, 383.
[33] R. J. Heath, J. R. Rubin, D. R. Holland, E. Zhang, M. E. Snow, C. O. Rock, *J. Biol. Chem.* **1999**, *274*, 11110.
[34] C. Baldock, J. B. Rafferty, A. R. Stuitje, A. R. Slabas, D. W. Rice, *J. Mol. Biol.* **1998**, *284*, 1529.
[35] H. P. Schweizer, *FEMS Microbiol. Lett.* **2001**, *202*, 1.
[36] B. D. Kalyon, U. Olgun, *Am. J. Infection Control* **2001**, *29*, 124.
[37] A.-H. Pei, Z.-W. Shen, G.-S. Yang, *Mater. Lett.* **2007**, *61*, 2757.
[38] L. Jin, A. H. Marcus, H. Miriam, F. G. Dale Jr., R. H. John, E. O. Paul, S. H. April, E. T. Alan, *J. Appl. Polym. Sci.* **2001**, *82*, 300.
[39] F. Maestrelli, P. Mura, M. J. Alonso, *J. Microencapsulation* **2004**, *21*, 857.
[40] S. M. Iconomopoulou, A. K. Andreopoulou, A. Soto, J. K. Kallitsis, G. A. Voyiatzis, *J. Controlled Release* **2005**, *102*, 223.
[41] S. Kockisch, G. D. Rees, J. Tsibouklis, J. D. Smart, *Eur. J. Pharmaceutics Biopharmaceutics* **2005**, *59*, 207.
[42] E. Pinon-Segundo, A. Ganem-Quintanar, V. Alonso-Perez, D. Quintanar-Guerrero, *Int. J. Pharm.* **2005**, *294*, 217.
[43] L. Qian, Y. Guan, H. Xiao, *Int. J. Pharm.* **2008**, *357*, 244.
[44] J.-C. Kim, M.-E. Song, E.-J. Lee, S.-K. Park, M.-J. Rang, H.-J. Ahn, *J. Dispersion Sci. Technol.* **2001**, *22*, 591.
[45] C. Antoine, J. P. Lellouche, J. Maclouf, P. Pradelles, *Biochim. Biophys. Acta* **1991**, *1075*, 162.
[46] C. Flesch, C. Delaite, P. Dumas, E. Bourgeat-Lami, E. Duguet, *J. Polym. Sci., Part A: Polym. Chem.* **2004**, *42*, 6011.
[47] A. Farkas, G. A. Mills, *Adv. Catal.* **1962**, *13*, 393.
[48] Y. Katsumoto, H. Komatsu, K. Ohno, *J. Am. Chem. Soc.* **2006**, *128*, 9278.
[49] L. T. Zhuravlev, *Colloids Surf. A* **2000**, *173*, 1.
[50] M. G. Escalada, J. L. Harwood, J. Y. Maillard, D. Ochs, *J. Antimicrobial Chemotherapy* **2005**, *55*, 879.
[51] C. Slater-Radosti, G. Van Aller, R. Greenwood, R. Nicholas, P. M. Keller, W. E. DeWolf, F. Fan, D. J. Payne, D. D. Jaworski, *J. Antimicrobial Chemotherapy* **2001**, *48*, 1.
[52] Y. Zhang, Y. Wu, M. Chen, L. Wu, *Colloids Surf. A* **2010**, *353*, 216.
[53] F. Pfluecker, J. Beck, B. Hirthe, S. John, N. Schulze, (Merck Patent GmbH, Sachtleben Chemie GmbH, Germany) *WO2006087066A1*, **2006**.
[54] C. Chen, N. Huang, T. Shimizu, (Toray Fibers & Textiles Research Laboratories China Co., Ltd., Peop. Rep. China) *CN101451275A*, **2009**.
[55] M. A. Correa-Duarte, M. Giersig, L. M. Liz-Marzán, *Chem. Phys. Lett.* **1998**, *286*, 497.
[56] T. J. Beveridge, *J. Bacteriol.* **1999**, *181*, 4725.
[57] J.-P. Lellouche, I. Makarovsky, Y. Boguslavsky, J. Lellouche, E. Banin, *patent 61/457,154*, **2011**.
[58] J. Lellouche, E. Kahana, S. Elias, A. Gedanken, E. Banin, *Biomaterials* **2009**, *30*, 5969.